Quantum creep and pinning properties of oxygen-deficient $YBa_2Cu_3O_{x_n}$ films

A. J. J. van Dalen* and R. Griessen

Free University, Faculty of Physics and Astronomy, De Boelelaan 1081, 1081 HV Amsterdam, The Netherlands

S. Libbrecht† and Y. Bruynseraede

Laboratorium voor Vaste-Stoffysica en Magnetisme, Katholieke Universiteit Leuven, Celestijnenlaan 200D, B-3001, Leuven, Belgium

E. Osquiguil

Centro Atómico, 8400 San Carlos de Bariloche, R. N. Argentina

A high sensitivity capacitance torquemeter has been used for a comprehensive investigation of the induced current densities and dynamic relaxation rates in a $YBa_2Cu_3O_{x_n}$ film with nominal oxygen content varying between $x_n = 6.55$ and $x_n = 7.0$. The dynamic relaxation rate Q does not extrapolate to zero at $T = 0$ K, indicating the presence of quantum creep. By changing the oxygen content of the film it is possible to investigate the relation between the quantum creep rate $Q(0)$ and the normal-state resistivity $\rho_n(0)$ at low temperature. Although $Q(0)$ increases monotonically with ρ_n, it is found that $Q(0)$ is not proportional to $\rho_n(0)$, in contrast to the predictions of a theory based on dissipative tunneling of collectively pinned single vortices [Blatter *et al.*, Rev. Mod. Phys. **66**, 1125 (1994)]. The experimental results imply that in $YBa_2Cu_3O_7$ quantum creep takes place in a transition regime between Hall tunneling and dissipative tunneling. For lower oxygen contents the quantum creep regime moves towards the dissipative limit. For each oxygen content the characteristic pinning energy $U_c(0)$ at $T = 0$ is obtained by a linear extrapolation to $T = 0$ K of the T/Q versus T curves. The critical current density j_c at $T = 0$ is determined independently by a linear extrapolation of the measured $\ln j_s$ versus T curves. A power-law relation $U_c(0) \propto [j_c(0)]^p$ with $p \approx 0.5$ is found, indicating single vortex pinning at higher temperatures. This is confirmed by a detailed analysis of the measured current densities and relaxation rates by means of the generalized inversion scheme developed by Schnack *et al.* [Phys. Rev. B **48**, 13 178 (1993)]. For $x_n \gtrsim 6.6$ at $B_e = 0.6$ T and for $x_n \gtrsim 6.7$ at $B_e = 2.0$ T the calculated temperature dependence of j_c and U_c agrees remarkably well with a model based on three-dimensional single vortex pinning caused by spatial fluctuations in the charge carrier mean free path. At lower oxygen contents and higher magnetic-fields the agreement gradually breaks down due to the increasing importance of thermal fluctuations. [S0163-1829(96)04925-9]

I. INTRODUCTION

Shortly after the discovery of the high-T_c superconductors it was observed[1] that the relaxation rate of the magnetic moment does not vanish as the temperature approaches $T = 0$ K. This contradicts the linear temperature dependence predicted by the Anderson-Kim model.[2] By using a nonlinear dependence of the activation energy $U(j)$ on the current density j, Griessen[3] showed that the relaxation rate approaches $T = 0$ K as $S \sim T^{1/n}$ with $n \geqslant 3/2$. However, this does not explain the observation that the relaxation rate becomes almost independent of temperature below $T \approx 1$ K as observed in many high-T_c superconductors, such as $YBa_2Cu_3O_7$,[4–8] $Bi_2Sr_2CaCu_2O_8$ and $Bi_2Sr_2Ca_2Cu_3O_{10}$ (Refs. 9–11), and $Tl_2Ba_2Ca_1Cu_2O_8$.[12,13]

The low-temperature saturation of the relaxation rate is indicative of quantum tunneling of vortices. Quantum creep of vortices in high-T_c superconductors has been studied theoretically by Blatter and co-workers.[14,15] They calculated the quantum creep rate in bulk superconductors by applying weak collective pinning theory. At low magnetic fields single vortices are individually pinned by the collective action of many weak pinning centers. Segments of a typical length L_c, which is called the correlation length, tunnel independently. At high magnetic fields the tunneling object is a collectively pinned vortex bundle.

On the basis of the prediction of Blatter *et al.*[15] for the creep rate in the single vortex limit, one expects that quantum creep will be favored in samples with a strong anisotropy, high normal-state resistivity, and a short coherence length. The purpose of this work is to make a quantitative test of the dissipative tunneling theory[14,15] by using samples with a relatively high normal-state resistivity at T_c which can unambiguously be extrapolated to low temperatures. For an optimal comparison we chose a single film of $YBa_2Cu_3O_{x_n}$ with various oxygen content. The advantage of working with one film is that only the effect of oxygen doping can be investigated since the addition and removing of oxygen can be done fully reversibly leaving the microstructure of the sample unchanged. As shall be shown below, the experimental results cannot be understood within a theory of purely dissipative tunneling. They can, however, be well explained by a theory which incorporates both dissipative and Hall drag terms.

Another purpose of this work is to investigate the relation between critical current density j_c and pinning in samples

with a variable concentration of weak pinning centers (oxygen vacancies). The induced current densities j_s and relaxation rates Q measured at sufficiently high temperature where the effects of quantum creep are negligible, are analyzed by means of the generalized inversion scheme (GIS) developed by Schnack et al.[16] in order to determine the *true* critical current density j_c and the characteristic pinning energy U_c. This method is based on the general assumption that the current dependence and the temperature dependence of the activation energy can be separated. Furthermore, one exploits the fact that a power law relates U_c and j_c. With this method it is possible to calculate the temperature dependence of j_c, which is in general clearly different from the measured current density j_s, and U_c, once the exponent p in the power-law relation $U_c \propto [j_c]^p$ is known. The GIS allows also to identify the pinning regime [single vortex (SV), small bundle pinning (SB), large bundle pinning (LB)] and the microscopic origin of the pinning (δT_c pinning due to spatial fluctuations in T_c or δl pinning due to spatial fluctuations in the mean free path of the charge carriers).

This paper is organized as follows. The theory of quantum creep of vortices, including dissipative tunneling and Hall tunneling, is briefly reviewed in Sec. II. The sample preparation and oxygen loading procedure is described together with the experimental technique used to measure the current density sample and its relaxation rate in Sec. III. An overview of the experimental results is given in Sec. IV. The relation between the low-temperature normal-state resistivity and the quantum creep rate is discussed in Sec. V A, whereas the magnetic-field dependence of the quantum creep rate is discussed in Sec. V B. The pinning properties of YBa$_2$Cu$_3$O$_{x_n}$ are considered in Sec. VI. A power-law relation between the characteristic pinning energy and the critical current density is found experimentally in Sec. VI A. The generalized inversion scheme is introduced and applied to measured data in Sec. VI B. The microscopic origin of pinning is discussed in Sec. VI C. The conclusions are given in Sec. VII.

II. THEORY OF QUANTUM CREEP

A. Dissipative quantum tunneling

At low temperatures the flux dynamics in high-T_c superconductors is governed by quantum creep of vortices through the pinning barriers. In contrast to thermally activated flux motion, this process is not only governed by the height of the pinning barrier but also by the time spent by the vortex segment under the barrier during the tunneling process.[14] Due to the coupling between the vortex and its environment, quantum creep is a dissipative process. The influence of the dissipation on the tunneling probability of a particle through a barrier has been evaluated by Caldeira and Legget.[17] The dissipative quantum creep relaxation rate Q_D can then readily be evaluated[18] to be

$$Q_D = A \frac{\hbar}{\eta x_{\text{hop}}^2} \frac{j_c}{j_s}, \tag{1}$$

where $2x_{\text{hop}}$ is the distance separating the metastable positions of the vortex segment before and after tunneling, η is the viscous drag coefficient, A is a numerical parameter of

order unity, j_c is the critical current for which the energy barrier between two vortex configurations vanishes, and j_s is the superconducting current induced in the sample by sweeping the external magnetic field at a certain sweep rate dB_e/dt. For $j_s \approx j_c$ and noting that x_{hop} is of the order of ξ, Eq. (1) becomes

$$Q_D \cong \frac{\hbar}{\eta \xi^2}. \tag{2}$$

Together with the Bardeen-Stephen expression[19] $\eta \cong \Phi_0 B_{c2} L_c / \rho_n(0)$ this leads to

$$Q_D \cong \frac{e^2}{2\hbar} \frac{\rho_n(0)}{L_c}, \tag{3}$$

where Φ_0 is the flux quantum, L_c is the length of the tunneling flux segment, and $\rho_n(0)$ is the normal-state resistivity at $T = 0$ K. Note that this result is, except for a numerical factor close to unity, identical to the result obtained from a collective pinning theory of single vortices derived by Blatter and co-workers.[14,15,20]

$$Q_D \cong \frac{e^2}{\hbar} \frac{\rho_n}{\epsilon \xi} \left(\frac{j_c}{j_0} \right)^{1/2}. \tag{4}$$

The relaxation rate does not depend on the orientation of the magnetic field and is identical for in-plane and out-of-plane motion, although the viscous drag coefficients and the elasticities of the vortex are different for these two types of motion. The c-axis correlation length $L_c \cong \epsilon \xi (j_0/j_c)^{1/2}$ is independent of angle and type of motion. Combining this result with Eq. (4) reproduces Eq. (3), which demonstrates that this formula remains valid in the anisotropic case.

B. Hall tunneling

Recently, Feigel'man et al.[21] proposed that high-T_c superconductors are not in the dissipative limit at low temperatures. Their analysis is, however, not based on a comparison of the kinetic and the dissipative terms in the Euclidean action describing the vortex motion. Instead of this, they estimate the electron mean free path l from a linear extrapolation of $\rho_n(T \gtrsim T_c)$ data which gives a low-temperature resistivity $\rho_n(0) \approx 10 \ \mu\Omega$ cm leading to $l \approx 70$ nm. This means that high-T_c superconductors might be in the superclean limit, satisfying the condition: $l \gg \xi(\epsilon_F/\Delta)$ in which ϵ_F is the Fermi energy and Δ is the energy gap. In this case, the flux motion has to be described by the following equation of motion:[22,23]

$$\eta \vec{v}_v + \alpha \vec{v}_v \times \hat{z} = \Phi_0 L_c \vec{j}_s \times \hat{z} + \vec{F}_{\text{pin}}, \tag{5}$$

where η and α are the viscous and the Hall drag coefficients, $\vec{v}_v$ is the vortex velocity, F_{pin} is the pinning force, and $\hat{z}$ a unit vector parallel to the vortex. Feigel'man et al.[21] use the analogy between vortex motion in a superconductor and nondissipative flow in helium-II to derive the following expression for the Hall drag coefficient:

$$\alpha = \pi \hbar n_s L_c, \tag{6}$$

where n_s is the density of superconducting electrons.[22] Finally, they calculate that the saddle-point solution of the Euclidean action S_E is given by

$$\frac{S_E^{\text{eff}}}{\hbar} \approx \frac{\alpha}{\hbar} V_c, \tag{7}$$

where V_c is the correlated volume of the vortex line segment or flux bundle. For a vortex line segment, this volume is approximated by $V_c \approx \xi^2 L_c$. This leads finally to the following expression for the dynamic Hall relaxation rate:

$$Q_H \approx \frac{\hbar}{\alpha \xi^2} \approx \frac{1}{\pi n_s \xi^2 L_c}. \tag{8}$$

Note that, in contrast to dissipative quantum creep, the Hall creep rate does *not* depend on the low-temperature normal-state resistivity $\rho_n(0)$. Measurements of the low-temperature relaxation rate $Q(0)$ at various values of the oxygen concentration x_n can be used to determine the character of quantum creep, since $\rho_n(0)$ increases markedly with decreasing x_n.

C. Interpolation between dissipative and Hall tunneling

The approaches to the problem of quantum creep of vortices in high-T_c superconductors given in the previous section are limited to the dissipative limit and the superclean (Hall) limit. A more general approach has recently been given by Stephen[24] for a parabolic potential of range x_c given by

$$U(x) = \frac{1}{2} k L_c x^2, \quad |x| \leq x_c,$$
$$\tag{9}$$
$$U(x) = -\infty, \quad |x| > x_c.$$

The Euclidean action S_E of the tunneling process is approximately related to the mean-square quantum fluctuation $\langle u_x^2 \rangle$ of the vortex position by[25]

$$S_E \approx \hbar \frac{x_c^2}{2\langle u_x^2 \rangle}. \tag{10}$$

For this model the mean-square fluctuation $\langle u_x^2 \rangle$ is given by[24]

$$\langle u_x^2 \rangle = \frac{\hbar \gamma}{2\pi k L_c} \int_0^{\omega_c} d\omega \frac{\omega \coth(\beta \hbar \omega/2)}{(\omega_0 - \omega)^2 + \gamma^2}, \tag{11}$$

where $\beta = 1/kT$ and ω_c is a cutoff frequency probably related to the superconducting gap energy. The parameters ω_0 and γ are given by

$$\omega_0 = \frac{\alpha k L_c}{\alpha^2 + \eta^2} \tag{12}$$

and

$$\gamma = \frac{\eta k L_c}{\alpha^2 + \eta^2}, \tag{13}$$

where α and η are the Hall drag and the viscous drag coefficients, respectively. As discussed by Kopnin and Salomaa[23] and Blatter *et al.*,[20] α and η depend on $\omega_B \tau$ as
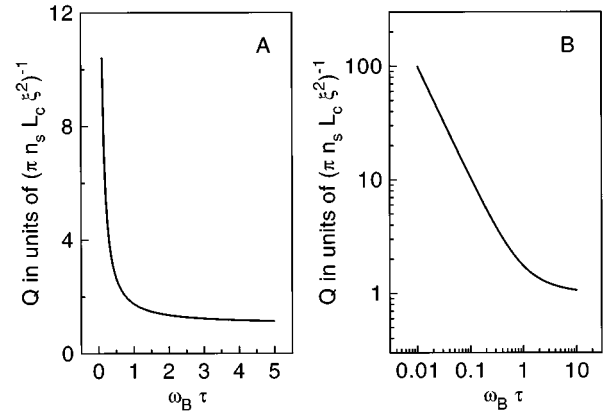

FIG. 1. Dependence of the quantum creep relaxation rate $Q(0)$ [in units of $(\pi n_s L_c \xi^2)^{-1}$] on $\omega_B \tau$ according to Eq. (17) derived from Stephen's treatment (Ref. 24) of vortex tunneling.

$$\alpha(\omega_B \tau) = \pi \hbar n_s L_c \frac{(\omega_B \tau)^2}{1 + (\omega_B \tau)^2} \tag{14}$$

and

$$\eta(\omega_B \tau) = \pi \hbar n_s L_c \frac{(\omega_B \tau)}{1 + (\omega_B \tau)^2}, \tag{15}$$

where the transport relaxation time is given by $\tau = m/n_s e^2 \rho_n(0)$. The energy separation $\hbar \omega_B$ between low-lying levels in the vortex core is approximately given by $\hbar \omega_B \approx \hbar e B_{c2}/m = \hbar^2/2m\xi^2$ where B_{c2} is the upper critical field. The quantum relaxation rate Q is inversely proportional to the Euclidean action, as outlined above. Together with Eq. (10) this leads to $Q \approx 2\langle u_x^2 \rangle / u_c^2 \approx 2\langle u_x^2 \rangle / \xi^2$, where we have used that the range of the pinning potential is approximately equal to ξ.

At sufficiently low temperatures, where the condition $k_B T \ll \hbar \omega_B$ is satisfied, we find from Eq. (11) after integration over the frequency ω

$$Q \approx \frac{\hbar}{S_E^{\text{eff}}} \approx \frac{1}{\pi n_s L_c \xi^2}$$
$$\times \left[\begin{array}{c} \frac{1}{2\pi\omega_B\tau} \ln\left\{ \frac{(\Omega_c - 1)^2(\omega_B \tau)^2 + 1}{(\omega_B \tau)^2 + 1} \right\} \\ + \frac{1}{\pi} \arctan\{(\Omega_c - 1)(\omega_B \tau)\} + \frac{1}{\pi} \arctan(\omega_B \tau) \end{array} \right],$$
$$\tag{16}$$

where $\Omega_c = \omega_c / \omega_B$. The expressions for the viscous drag coefficient and the Hall coefficient given above have been used in the derivation of this result. The logarithmic term is only weakly dependent on $\omega_B \tau$ and will be approximated by a constant, leading to

$$Q(T=0, \omega_B \tau) \approx \frac{1}{\pi n_s L_c \xi^2} \left[\frac{1}{\omega_B \tau} + \frac{1}{2} + \frac{1}{\pi} \arctan(\omega_B \tau) \right]. \tag{17}$$

The function $f(\omega_B \tau)$ between square brackets in Eq. (17) is plotted in Figs. 1(a) and 1(b). From these figures it follows that $f(\omega_B \tau)$ has the interesting property to be essentially

constant and equal to 1 for $\omega_B \tau > 1$. In the dissipative limit $\omega_B \tau \ll 1$ we recover Eq. (3), whereas in the pure Hall limit $\omega_B \tau \gg 1$, Eq. (17) reduces to Eq. (8).

III. EXPERIMENTAL METHODS

A. Sample preparation

The YBa$_2$Cu$_3$O$_{x_n}$ (YBCO) film is prepared using *in situ* 90° off-axis magnetron dc sputtering from a single stoichiometric YBCO target. During sputtering the total chamber pressure is 400 mTorr, the gas is an 80% Ar/20% O$_2$ mixture and the MgO (100) substrate is at a temperature of 740 °C. X-ray diffraction as well as Rutherford backscattering spectroscopy channeling measurements show that the film is grown epitaxially on the MgO (100) substrate, with a channeling minimum yield smaller than 7%. The layers are purely *c*-axis oriented and have narrow rocking curves [full width at half height (005) $\leq 0.3°$]. This *in situ* prepared film has a $T_c(R=0) = 89$ K and a transition width of 1 K. The critical current density J_c at an applied field $B = 0.5$ T is 2×10^{11} A/m^2 at 4.2 K and 4×10^8 A/m^2 at 77 K determined with torque magnetometry. The thickness of the film is 450 nm which is inferred from the sputtering time and the growth rate. More details about the preparation and characterization have been published elsewhere.[26]

The oxygen content of the film is adjusted to the desired value by using the oxygen pressure-temperature $(P_{O_2} - T)$ phase diagram.[27] In order to reduce the oxygen content in a controlled way, the sample is inside a stoichiometric YBCO ceramic box. Starting in an oxygen atmosphere of 10 Torr (1.33 kPa) at an annealing temperature $T_{ann}(x_n)$, $[T_{ann}(x_n)$ varying between 435 °C for $x_n = 6.9$ and 545 °C for $x_n = 6.65]$ the film is slowly cooled down (2–3 °C/min), while the O$_2$ pressure is decreased in order to follow the corresponding oxygen content line in the $(P_{O_2} - T)$ phase diagram.[28] Finally, the film is quenched to room temperature in $P(O_2) \approx 75$ mTorr (10 Pa) and from a quench temperature $T_q(x_n)$ varying between $T_q = 360$ °C for $x_n = 6.9$ and $T_q = 444$ °C for $x_n = 6.65$. Before each oxygen content changing procedure, the film is fully oxidized by annealing it during 15–30 min at $T=500$ °C and $P(O_2) = 750$ Torr (100 kPa). After four oxygen treatments the T_c of the fully oxydized film has decreased with approximately 1 K, which indicates that the oxygen depletion process is very reproducible. Furthermore, this small decrease of T_c demonstrates that the quality of the sample is only weakly influenced by the oxygen treatments.

B. Oxygen content and the normal-state resistivity

Figure 2 shows the resistivity versus temperature for the YBa$_2$Cu$_3$O$_{x_n}$ film with different nominal oxygen contents x_n, as used in the torque measurements described below. The resistivity of the film is measured with a standard dc four-probe technique using wire bonding contacts. After each resistance measurement the contacts are removed from the sample. The film has a sharp transition when it is fully loaded with oxygen, whereas the transitions become broader as the oxygen content is lowered. The transition is unusually broad if the oxygen content is lowered to $x_n=6.55$, which
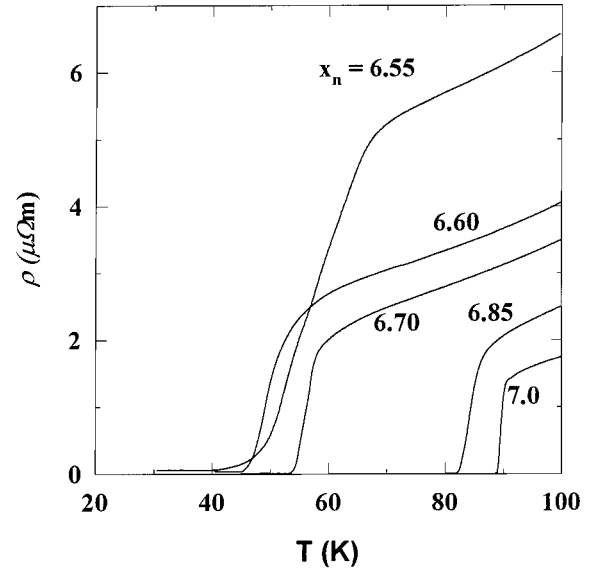

FIG. 2. Resistivity measurements for several oxygen contents of the 450 nm YBa$_2$Cu$_3$O$_{x_n}$ film used in the torque experiments. At high oxygen content the extrapolation to $T=0$ K of the resistivity is close to zero, whereas a clear and unambiguous nonzero value is obtained at low oxygen content. The large width of the transition for $x_n = 6.55$ is due to inhomogeneities in the oxygen concentration due to the large thickness of the sample.

indicates an inhomogeneous oxygen distribution in the film. This is probably due to the rather large thickness, 450 nm, of the film used in this work.

The critical temperature T_c at 5% of the transition is shown as a function of the oxygen content in Fig. 3. For comparison the plot also contains data on two other YBa$_2$Cu$_3$O$_{x_n}$ films produced with the same method. These T_c values were obtained with a superconducting quantum interference device (SQUID) magnetometer and an ac susceptometer.[29] The T_c values obtained from the films are in good agreement with the data from bulk samples. In con-
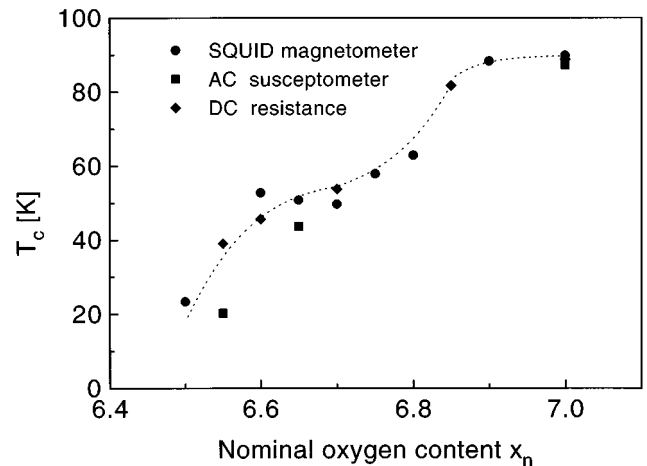

FIG. 3. Oxygen content dependence of the critical temperature T_c of YBa$_2$Cu$_3$O$_{x_n}$ films. The plot contains data obtained by means of a SQUID magnetometer (Ref. 29), ac susceptometer (Ref. 29), and the resistively determined T_c values of the film used in this work.
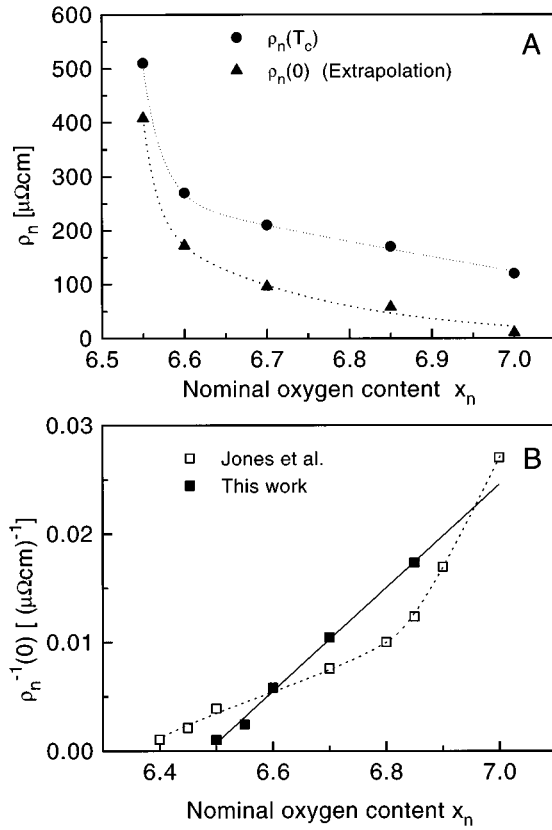
FIG. 4. (a) Oxygen content dependence of the normal-state resistivity $\rho_n(0)$ at zero temperature, obtained by extrapolation from $\rho_n(T)$ measured at $T>T_c$. The normal-state resistivities at $T=T_c$ are shown for comparison. (b) Inverse low-temperature resistivity as a function of the oxygen content. The solid line is a linear fit to our data, whereas the dotted line through the data of Jones *et al.* (Ref. 31) is a guide to the eye.

trast to the observation of Osquiguil *et al.*[27] the films show two distinct plateaus in the T_c versus x_n curves. The T_c values of Fig. 3 are in good agreement with values obtained by Ossandon *et al.*[30] who performed an absolute determination of the oxygen content x by using a thermogravimetric analysis system.

In order to compare the observed quantum creep rates with the theoretical predictions given in the previous section, it is necessary to determine the normal-state resistivity $\rho_n(0)$ at low temperatures. A linear extrapolation to $T=0$ K of the measured resistivity leads to a value $\rho_n(0)\approx10$ $\mu\Omega$ cm for the fully oxydized film. However, it is far from certain that this linear extrapolation is valid. Fortunately, this problem disappears when the nominal oxygen content is lowered. The extrapolation of the $\rho_n(T)$ curves to $T=0$ K becomes less ambiguous, because T_c is lowered, $\rho_n(T_c)$ is increased, and the curves develop a clear upward curvature. Resistivity values at $T=0$ K obtained from extrapolations are shown in Fig. 4(a) together with the resistivity $\rho_n(T_c)$ at $T=T_c$. The inverse of $\rho_n(0)$, which is proportional to the electron scattering time τ is shown as a function of the oxygen content in Fig. 4b, together with results obtained by Jones *et al.*[31] The observed linear variation of our $[\rho_n(0)]^{-1}$ data suggests that $\rho_n(0)=41\mu\Omega$ cm for $x_n=7.0$. Note that this value is in good agreement with

$\rho_n(0)=37\mu\Omega$ cm for fully oxydized $YBa_2Cu_3O_7$ obtained by Jones *et al.* For the presentation of experimental results we shall use $\rho_n(0)=41\mu\Omega$ cm in the remaining part of this paper.

C. Torque magnetometry

The capacitance torquemeter used in this work is similar to that used in Ref. 32 and consists of two parallel capacitor plates, connected by phosphorus bronze springs. The base plate is attached firmly to a revolving sampleholder, while the detection plate which carries the sample moves freely. A torque exerted on this detection plate rotates it over a small angle $\delta\theta$ towards a new equilibrium position. This angular displacement and the corresponding change in capacitance are proportional to the torque, because the springs obey Hooke's law. The torque magnetometer is calibrated by means of a small coil through which a known current is passed.

For the conversion of magnetic moment into induced current density it is assumed that a homogeneous current distribution is set up in the sample. This seemingly crude assumption is justified by magneto-optical experiments of Koblischka *et al.*[33] and Schuster *et al.*[34] and more recently by Koblischka *et al.*[35] Furthermore its validity has also been shown by numerical calculations of Schnack *et al.*[36] and Brandt.[37] These calculations show that the flux profile remains virtually linear during conventional relaxation.

A homogeneous current distribution in a rectangular sample leads to the following expression for the magnitude of the magnetic moment $\mathcal{M}$:[38]

$$\mathcal{M}=\frac{1}{4}a^2d(b-a/3)j_s, \quad b\geqslant a, \quad (18)$$

where a and b are the lengths of the sides of the sample, d is the thickness of the sample along the c axis, and j_s is the current density flowing through the entire sample. In the derivation of this equation it has been assumed that the current flows in the ab plane. This is justified by the geometry of the sample $d\ll a,b$ and also because $j_c^{ab}\gg j_c^c$.

The experiments were performed in the bore of a 7 T Oxford Instruments superconducting NbTi magnet mounted in a low-loss helium cryostat. Temperature control and stabilization within 0.1 K is realized by simultaneously regulating the flow of liquid helium through the heat exchanger and the voltage supplied to a heater coil. In contrast to a conventional flow cryostat the liquid helium necessary for the temperature regulation is taken from an internal reservoir which is also used for cooling the magnet.

In this work the dynamic relaxation rate

$$Q\equiv d\ln j_s/d\ln(dB_e/dt) \quad (19)$$

is determined from measurements of j_s at various sweep rates dB_e/dt of the magnetic field. As shown by Jirsa *et al.*[39] and Pŭst *et al.*[40] the dynamic relaxation rate Q is closely related to the conventional relaxation rate $R\equiv-d\ln\mathcal{M}/d\ln t$ where $\mathcal{M}$ is the magnetic moment of the sample. This observation is supported by numerical calculations by Schnack *et al.*[36]
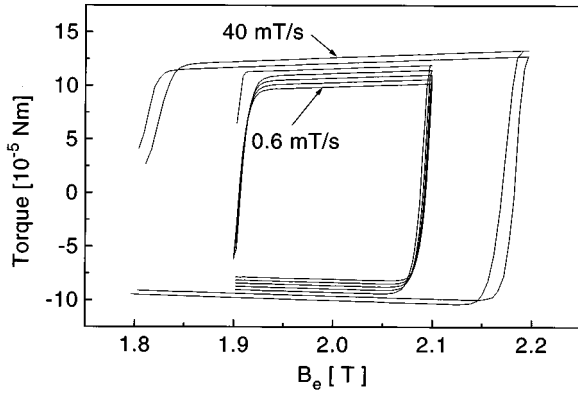
FIG. 5. Minor torque hystersis loops measured at $T=15$ K and $B_e=2.0$ T on $YBa_2Cu_3O_{x_n}$ with $x_n=6.85$. The magnetic-field sweep rates used here are $dB_e/dt=40$ (outer curve), 20, 10, 5, 2.5, 1.25, and 0.6 (inner curve) mT/s, respectively. The torque and thus the induced current density j_s increases linearly with $\ln(dB_e/dt)$.

Minor hysteresis loops (MHL) have been made around central field values $B_e=0.6$ T, $B_e=2.0$ T, and $B_e=6.9$ T, respectively. The width of the loops has been chosen large enough to fully penetrate the sample to make sure that it is in the critical state at the field where the width of the hysteresis loop is measured. MHL's have been recorded at sweep rates $dB_e/dt=0.6$, 1.25, 2.5, 5, 10, 20, and 40 mT/s.

IV. EXPERIMENTAL RESULTS

An example of MHL's is shown in Fig. 5. During these measurements the temperature was stabilized at 15 K. The oxygen content of the $YBa_2Cu_3O_{x_n}$ sample was 6.85 in this case. Apart from the steep slopes at the edges of the MHL's, the torque and also the magnetic moment and the average induced current density are only weakly dependent on the field. This indicates that the sample has reached the critical state during the MHL's. We checked that a large hysteresis loop from $B_e=0$ T to $B_e=7$ T and back gives the same value for the hysteresis at the same field and sweep rate as used in the MHL. The hysteresis loops tend to merge with a common curve directly after the reversal of the field sweep direction. The magnetic moment thus becomes independent on dB_e/dt, indicating that the sample is evolving from one critical state into the other one.

From Fig. 5 it is clear that the torque hysteresis and thus the average induced current density j_s is reduced by the same amount whenever the sweep rate is lowered by a factor of 2. This shows that j_s varies linearly with $\ln(dB_e/dt)$ and that the relaxation rate Q is only weakly dependent on the sweep rate. We have determined Q as a function of temperature and external field for samples with nominal oxygen contents $x_n=6.55$, $x_n=6.6$, $x_n=6.7$, $x_n=6.85$, and $x_n=7.0$, respectively.

The dynamic relaxation rate is displayed in Figs. 6(a), 6(b), and 6(c) for $B_e=0.6$, 2, and 6.9 T, respectively, and all oxygen contents mentioned above. It is clear that the relaxation rate does not extrapolate to zero at $T=0$ K, but remains finite. The nonzero extrapolation $Q(0)$, which is attributed to quantum creep, increases with decreasing oxygen content. This is shown in more detail in Fig. 7 from which one also
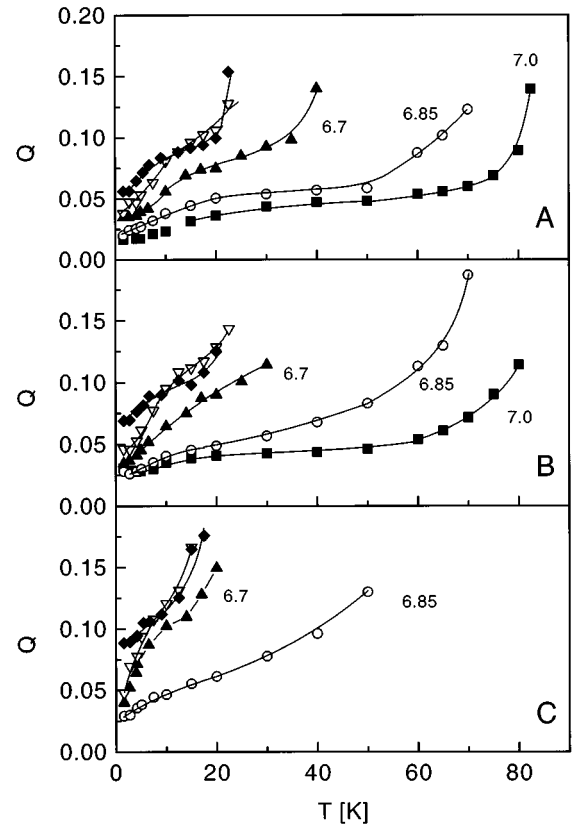

FIG. 6. Temperature dependence of the dynamic relaxation rate Q measured at $B_e=0.6$ T (a), 2.0 T (b), and 6.9 T (c). Each graph contains the data for the various oxygen contents x_n used in this work. The data for $x_n=6.55$ (filled diamond) and $x_n=6.6$ (open triangle) overlap.

observes that the quantum creep rate increases with increasing field.

Furthermore, the width of the hysteresis loops is used to obtain j_s. Values of j_s obtained at $B_e=0.6$, 2, and 6.9 T, are shown in Figs. 8(a), 8(b), and 8(c), respectively. For all x_n
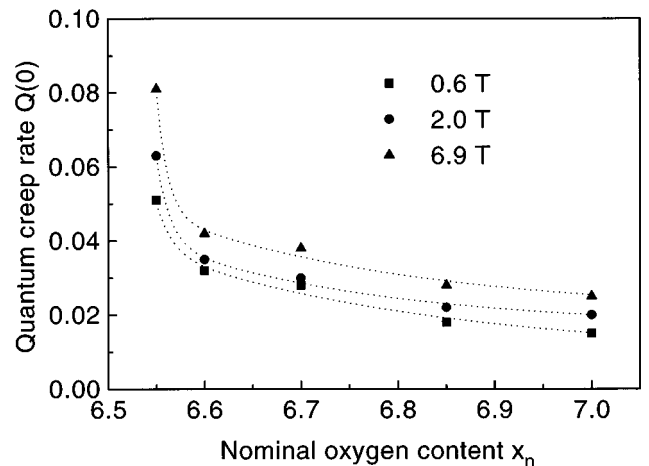

FIG. 7. Quantum creep rate $Q(0)$ of a 450 nm $YBa_2Cu_3O_{x_n}$ film as a function of the nominal oxygen content x_n and the applied magnetic field. The quantum creep rate has been obtained by an extrapolation in Fig. 6 of the measured temperature dependence of the relaxation rate $Q(T)$ to $T=0$ K.
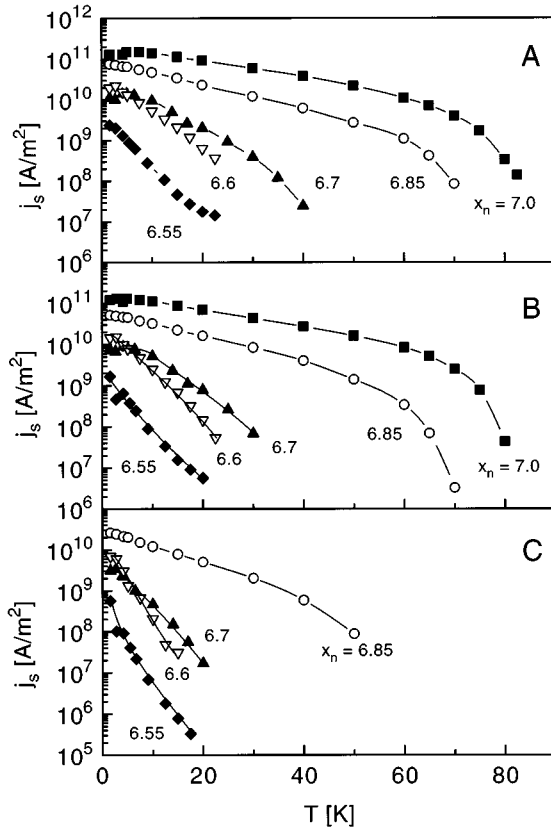
FIG. 8. Temperature dependence of the induced current density j_s, measured at a sweep rate $dB_e/dt = 40$ mT/s. The applied magnetic-field is $B_e = 0.6$ T (a), 2.0 T (b), and 6.9 T (c). Each graph contains the data for the various oxygen contents x_n used in this work.

the current density decreases approximately exponentially with temperature, except at low temperatures ($T < 10$ K) and at high temperatures close to the irreversibility line. The deviation at high temperatures is caused by thermal depinning whereas the saturation at low temperatures is due to quantum creep.[41] Extrapolation of the linear part of the lnj_s versus T curve leads to $j_s(0)$ which is the current density that would be observed in the absence of quantum creep. There is no thermally activated flux motion at $T = 0$ K and therefore $j_s(0)$ is equal to the critical current density j_c defined by the condition that the activation energy $U = U(j_s, T, B_e)$ for thermal hopping of vortices vanishes for $j_s = j_c$, i.e., $U(j_c, T, B_e) = 0$. The values for $j_s(0)$ are shown in Fig. 9 as a function of the oxygen content for $B_e = 0.6$ and 2.0 T.

V. QUANTUM CREEP IN YBa$_2$Cu$_3$O$_{x_n}$

A. Quantum creep and the role of the normal-state resistivity

Since Eqs. (3) and (4) predict that $Q(0)$ is proportional to the normal-state resistivity $\rho_n(0)$ at low temperatures, we have plotted in Fig. 10 $Q(0)$ versus the normal-state resistivity values shown in Fig. 4(b) with $\rho_n(0) = 41\mu\Omega$ cm for $x_n = 7.0$ as discussed above. We observe that $Q(0)$ increases approximately linearly with $\rho_n(0)$, but with a finite intercept at low resistivities. At first sight one could try to explain this by claiming that the c-axis correlation length L_c depends on
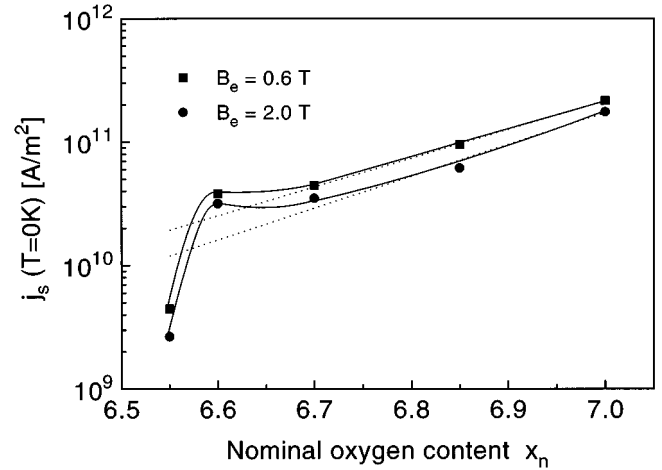

FIG. 9. Oxygen content dependence of the critical current density $j_s(0)$ at $T = 0$ K and $B_e = 0.6$ T and 2.0 T. The $j_s(0)$ values are determined by a linear extrapolation to $T = 0$ K of the observed linear temperature dependence of ln$j_s(T)$.

the oxygen content, since $Q \propto L_c^{-1}$. Published values for λ, ξ,[30,42] and γ[43] indeed show a strong dependence on the oxygen content. For clarity, the values of λ, ξ, and γ as a function of the oxygen content are shown in Figs. 11(a), 11(b), and 11(c), respectively. However, the ratio $\lambda/\xi^{1/2}$, which is inversely proportional to L_c, is only very weakly dependent on x_n, as can be seen in Fig. 11(d). Although the values found by Ossandon *et al.*[30] are somewhat higher than the values from Gray *et al.*,[42] the ratios $\lambda/\xi^{1/2}$ are in good agreement with each other. Therefore we take $\lambda/\xi^{1/2} = 1.2 \times 10^2$ nm$^{1/2}$, independent of the oxygen content. The independence of $\lambda/\xi^{1/2}$ on x_n is confirmed by measurements of λ and ξ by Däumling.[44] Their data are more scattered, but there is no significant change of $\lambda/\xi^{1/2}$ if x_n ranges from 6.5 to 7.0.

The increase of the anisotropy parameter γ with decreasing x_n is almost completely compensated by the decrease of
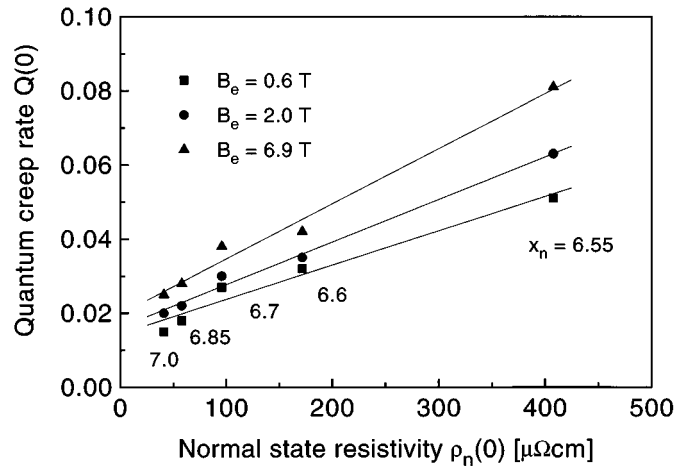

FIG. 10. Quantum creep rate $Q(0)$ of a 450 nm YBa$_2$Cu$_3$O$_{x_n}$ film displayed as a function of the low-temperature normal-state resistivity $\rho_n(0)$ at $B_e = 0.6$ T, 2.0 T, and 6.9 T. The corresponding values of the nominal oxygen content are indicated in the graph. The solid lines are linear fits to the data. Note that these lines do not extrapolate to $Q(0) = 0$ at $\rho_n = 0$ $\mu\Omega$ cm.
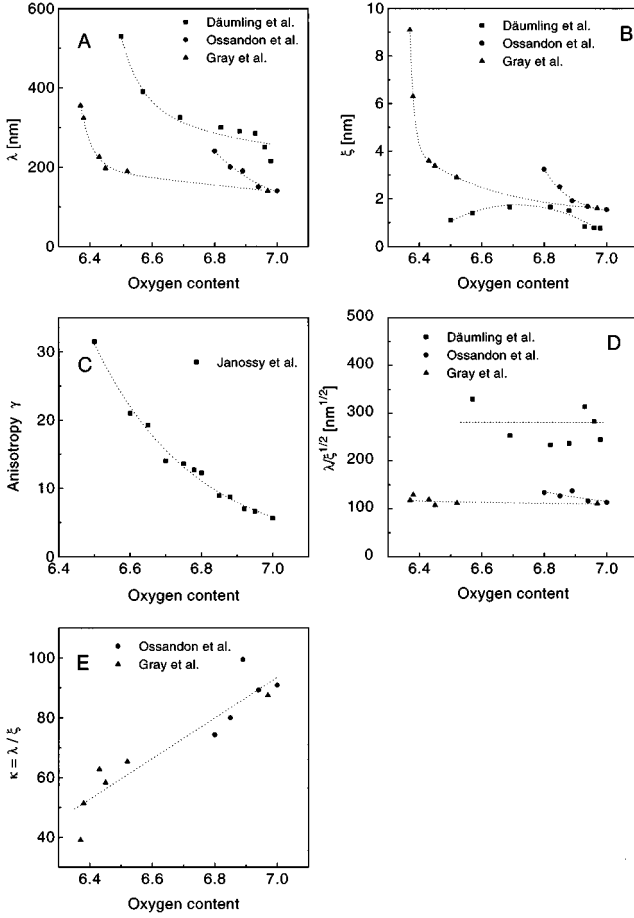
FIG. 11. Oxygen content dependence of the penetration depth λ (a), the coherence length ξ (b), and the anisotropy parameter $\gamma=(M/m)^{1/2}=\lambda_c/\lambda_{ab}$ (c). The oxygen content dependence of the ratio $\xi^{1/2}/\lambda$ (d) and the Ginzburg-Landau parameter $\kappa=\lambda/\xi$ (e) have been calculated from these data. The dotted lines in this figure are a guide to the eye.

TABLE I. Coherence length, penetration depth, anisotropy, critical current density extrapolated to $T=0$ K, and correlation length as a function of the oxygen content.

x_n	ξ (nm)	λ (nm)	γ	j_c (A/m^2)	L_c (nm)
7.0	1.60	146	5.6	2.16×10^{11}	2.6
6.85	1.93	160	9.3	9.53×10^{10}	2.3
6.7	2.43	180	15.6	4.46×10^{10}	2.0
6.6	2.80	193	22.1	3.83×10^{10}	1.5
6.55	3.06	202	26.6	4.47×10^{9}	3.6

on the oxygen content. The values for L_c obtained from Eq. (20) and the experimental data described above are given in Table I.

From Eqs. (3) and (4) and the weak variation of L_c with oxygen content follows that the quantum creep rate should be proportional to the normal-state resistivity in the purely dissipative limit. From Fig. 10 it can be seen that the quantum creep rate increases approximately linearly with the normal resistivity. However, the quantum creep rate is not proportional to the normal-state resistivity $\rho_n(0)$, since there is a finite intercept at low resistivities. *This leads to the important conclusion that the vortex system in oxygen-deficient YBa$_2$Cu$_3$O$_{x_n}$ cannot be in a purely dissipative limit since a finite intercept is in contradiction with Eq. (3).*

An estimate of $\omega_B\tau$ and thus a determination of the nature of the vortex motion can be obtained from a comparison of the measured quantum creep rates $Q(0)$ with the Stephen interpolation formula in Eq. (17). From $n_s \propto \lambda^{-2}$ follows that the prefactor on the right-hand side of Eq. (17) varies as $\kappa^2=\lambda^2/\xi^2$. Together with the measured quantum creep rates $Q(0)=0.02$ at $x_n=7.0$ and $Q(0)=0.063$ at $x_n=6.55$ and $B_e=2$ T it follows that the function f between the square brackets in Eq. (17) increases by a factor of 6 upon oxygen removal. The change of $\omega_B\tau$ upon oxygen removal can be evaluated from the variation of $\rho_n(0)$ and κ with oxygen content. This leads to the observation that $\omega_B\tau$ increases by a factor of 19 when the oxygen content decreases from $x_n=7.0$ to $x_n=6.55$. The values of $\omega_B\tau(x_n=6.55)$ and $\omega_B\tau(x_n=7.0)$ can be found by simultaneously solving

$$f(\omega_B\tau(x_n=6.55))/f(\omega_B\tau(x_n=7.0))=6,$$
$$\omega_B\tau(x_n=7.0)=19\times\omega_B\tau(x_n=6.55). \tag{21}$$

This leads to $\omega_B\tau(x_n=6.55)=0.14\pm0.01$ and $\omega_B\tau(x_n=7.0)=2.6\pm0.2$. Repeating this procedure at $B_e=0.6$ T and $B_e=6.9$ T leads within experimental error to the same estimates for $\omega_B\tau(x_n=6.55)$ and $\omega_B\tau(x_n=7.0)$.

An upper estimate for $\omega_B\tau(x_n=6.55)$ follows from the observation that the function f between square brackets in Eq. (17) increases with a factor of 6 upon oxygen removal. Using the fact that $f(\omega_B\tau)>1$ for all values of $\omega_B\tau$, one sees from Fig. 1 that in the extreme case where $\omega_B\tau(x_n=7.0)$ would be infinite, then $\omega_B\tau(x_n=6.55)$ would need to be 0.18 in order to have a factor of 6 between the values of the function f. This leads to the condition $\omega_B\tau(x_n=6.55)\lesssim0.18$.

This analysis can be performed in a more accurate way by fitting the measured quantum creep rates to the interpolation

the current density $j_s(0)=j_c$. Furthermore, the variation of $\sqrt{\ln\kappa}$ is approximately 5% and thus not of major importance. For the evaluation of L_c, we use that L_c is given by[15]

$$L_c\approx\left(\frac{\Phi_0}{4\pi\lambda^2}\frac{\epsilon^2}{\mu_0}\frac{\xi}{j_c}\ln\kappa\right)^{1/2}\approx\epsilon\xi(j_0/j_c)^{1/2}, \tag{20}$$

where $j_0=\Phi_0/3\sqrt{3}\pi\mu_0\lambda^2\xi$ is the depairing current density. However, this equation is only valid in the single vortex regime. An extensive proof that YBa$_2$Cu$_3$O$_{x_n}$ is in the single vortex regime, for all oxygen contents used, even at $B_e=7$ T is given below. Because the critical current density is at most weakly field dependent in the single vortex regime, we have used the current density $j(0)$ obtained at $B_e=0.6$ T, which is the lowest field value used in the experiment, to evaluate L_c. Furthermore, the use of field-dependent values of $j_c(0)$ for the evaluation of L_c would lead to an increase of L_c with increasing field. Together with the fact that according to Eq. (3) the quantum creep rate is proportional to $(L_c)^{-1}$ in the single vortex regime, this would predict that $Q(0)$ decreases with increasing field. This is in contradiction with the measured data displayed in Fig. 10. This leads finally to a correlation length which is only weakly dependent
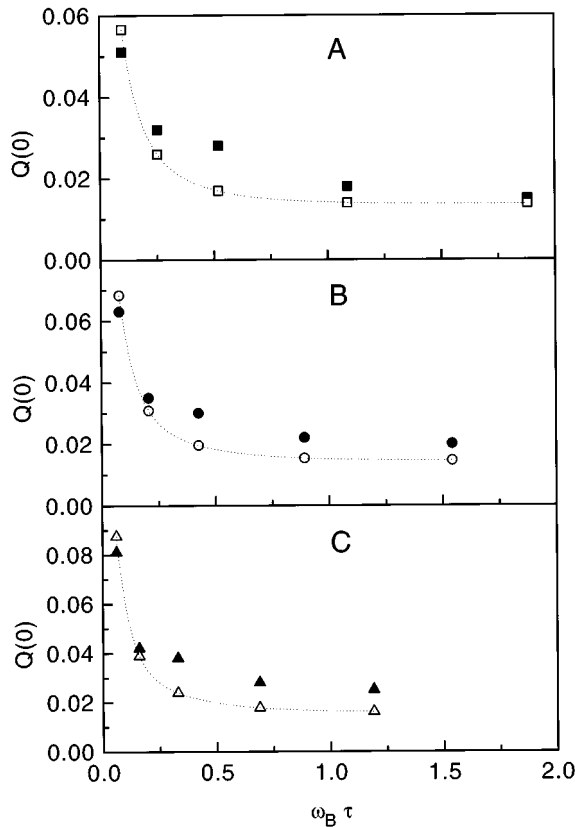
FIG. 12. Comparison between measured quantum creep rates $Q(0)$ and the values of $Q(0)$ obtained from a fit of the experimental data with Eq. (17) for $B_e = 0.6$ T (a), 2.0 T (b), and 6.9 T (c). The full symbols correspond to measured $Q(0)$ values, while the open symbols correspond to calculated values.

formula, Eq. (17). The values of $\omega_B \tau$ determined from the expressions for ω_B and τ given above, which lead to

$$\omega_B \tau = \frac{\hbar}{2e^2 n_s \xi^2 \rho_n(0)}, \qquad (22)$$

are multiplied by a fixed number, which is treated as a fitting parameter.

The results of this fitting procedure are shown in Fig. 12. The closed symbols represent the measured quantum creep rates, whereas the open symbols represent the fitted values. It is important to note that the fitted values of the creep rate do not simply fall on a single function $f(\omega_B \tau) = 1/(\omega_B \tau) + 1/2 + 1/\pi \arctan(\omega_B \tau)$, due to the variance of $n_s \xi^2$ with the oxygen content. The values of $\omega_B \tau$ found by this fitting procedure are consistent with the estimates mentioned above. In summary, we find that oxygen-deficient $YBa_2Cu_3O_{x_n}$ with $x_n = 6.55$ is close to the dissipative limit, whereas fully oxygenated $YBa_2Cu_3O_7$ is in the intermediate regime between Hall and viscous vortex motion. This conclusion is further supported by the fact that quantum creep in $YBa_2Cu_3O_7/PrBa_2Cu_3O_7$ multilayer systems also occurs in this intermediate regime.[45]

B. Magnetic-field dependence of the quantum creep rate

From Fig. 10 it is obvious that the quantum creep rate increases slightly with increasing field for oxygen contents

down to $x_n = 6.55$. In the single vortex limit, the quantum creep rate as well as the critical current density should not depend on the average distance between the vortices, since in this case they move independently. However, it is still possible that the correlation length of the tunneling vortex segment is field dependent due to a field-dependent anisotropy.

In the Ginzburg-Landau theory the anisotropy is independent of field and temperature. This is in contrast with the behavior of a stack of Josephson coupled superconducting layers for which Daemen *et al.*[46] have demonstrated that the anisotropy increases as the magnetic field increases due to the field dependence of the c-axis penetration depth λ_c. An increase of the anisotropy leads to a shorter correlation length and consequently to a larger quantum creep rate, which has been observed on bulk and powdered $Bi_2Sr_2Ca_2Cu_3O_{10}$ compound samples by Moehlecke and Kopelevich.[9] Therefore, the observed increase of the quantum creep rate with increasing field does not necessarily contradict single vortex pinning in three dimensions.

In the case of tunneling of two-dimensional (2D) vortex pancakes the correlation length is equal to the distance between the CuO planes which is, of course, inherently field independent. This leads to a field-independent quantum creep rate which has been observed in the highly anisotropic materials $Bi_2Sr_2CaCu_2O_8$ (Refs. 10 and 11) and $Tl_2Ba_2Ca_1Cu_2O_8$.[12,13]

At high magnetic fields where the vortices form (super) bundles the quantum creep rate decreases with increasing field. This is caused by a growth of the flux bundle and therefore an increased activation energy and Euclidean action as the field increases. For small bundles the quantum creep rate depends on the magnetic field as $Q(0) \propto B_e^{-1/2} \exp(-B_e^{3/2})$ whereas for large bundles[14,20] $Q(0) \propto B_e^{-13/2}$. This rather strong decrease of $Q(0)$ with increasing field is in contrast with the results shown in Fig. 10. This means that the increase of the quantum creep rate cannot be explained by pinning of flux (super)bundles, neither in the local limit (small bundles), nor in the nonlocal limit (large bundles). This indicates that in the field regime investigated in this work quantum creep occurs in the single vortex limit. Furthermore, the crossover field B_{sb} separating single vortex pinning and small bundle pinning is determined by the condition $L_c = \gamma^{-1} a_0$ where $a_0 = (\Phi_0/B_{sb})^{1/2}$ is the average distance between the vortices. Together with $L_c \approx 2.5$ nm and $\gamma = 5.6$ for $x_n = 7.0$ this gives $B_{sb} \approx 11$ T, confirming that for $YBa_2Cu_3O_7$ quantum creep takes place in the single vortex limit. However, due to the increase of the anisotropy with decreasing oxygen content, B_{sb} shifts to lower values and for $x_n = 6.55$, $\gamma = 26$ leads to $B_{sb} \approx 0.5$ T. This would imply that for $YBa_2Cu_3O_{x_n}$ with reduced oxygen content, the tunneling object is not a single vortex segment but a vortex bundle. This is not consistent with the observed weak increase of $Q(0)$ with increasing field.

VI. PINNING PROPERTIES OF $YBa_2Cu_3O_{x_n}$

In this section we discuss the relaxation data by means of two different approaches. First, in Sec. VI A we use a collective pinning theory which assumes a particular current dependence of the activation energy. This approach, which is certainly not adequate for the entire temperature range, can

TABLE II. Theoretical exponents μ and p as a function of the pinning regime and dimensionality.

Pinning regime	μ	μ	p	p
Dimensionality	3	2	3	2
Single vortex	1/7		1/2	1
Small bundles	3/2	8/9	−3/2	−1/2
Large bundles	7/9	1/2	−1/2	0

be used to determine values of the characteristic activation energy U_c at low temperature. In a second approach we use the generalized inversion scheme of Schnack (GIS) *et al.*[16] to determine the temperature dependence of U_c and the *true* critical current density j_c.

A. Current-dependent activation energy

For intermediate temperatures the flux motion in the $YBa_2Cu_3O_{x_n}$ film is well described in terms of thermally activated vortex hopping. The central parameter in this theory is the activation energy $U(j,T,B_e)$ the flux line or flux bundle has to overcome in order to move from a given configuration to an adjacent metastable pinning configuration. The influence of the current density j on the activation energy has been investigated theoretically by Feigel'man *et al.*[47] for the case of vortices (or vortex bundles) pinned by the collective action of randomly distributed weak pinning centers. They followed a scaling approach to obtain the size of the tunneling object. Together with the free-energy functional, this leads finally to a power-law relation $U(j) \propto j^{-\mu}$. Since $U(j)$ should vanish for $j=j_c$ it is now general practice to use the following interpolation relation:

$$U(j) = \frac{U_c}{\mu}\left[\left(\frac{j_c}{j}\right)^{\mu} - 1\right]. \quad (23)$$

This equation contains the linear[2] ($\mu = -1$) and the logarithmic current dependence[48] ($\mu = 0$) as special cases. The value of the exponent μ is determined by the pinning regime (single vortex, small bundles, or large bundles) and the dimensionality of the system. Theoretical values of μ are given in the left-hand part of Table II.

Using the fact that during a sweep of the applied magnetic field the activation energy[36] is given by $U(j_s,T,B_e) = CkT$, where for a disk-shaped sample $C = \ln(2v_0 B_e / R(dB_e/dt))$ in which v_0 is an attempt velocity and R is the radius of the sample, one can evaluate the ratio j_s / j_c using Eq. (23) leading to

$$j_s = j_c\left[1 + \frac{\mu kT}{U_c}\ln\left(\frac{2v_0 B_e}{RdB_e/dt}\right)\right]^{-1/\mu}. \quad (24)$$

From this equation the dynamic relaxation rate $Q = d\ln j_s / d\ln(dB_e/dt)$ can be calculated by taking the normalized derivative of j_s with respect to $\ln(dB_e/dt)$. Finally, by using the expression for C given above, one finds[49]

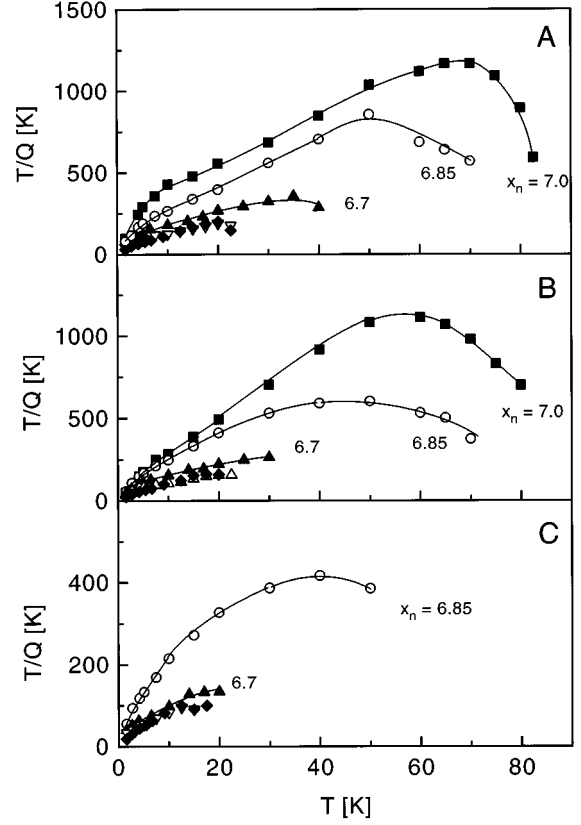$$\frac{T}{Q} = \frac{U_c}{k} + \mu CT, \quad (25)$$

FIG. 13. Temperature dependence of T/Q in an oxygen-deficient $YBa_2Cu_3O_{x_n}$ film measured at $B_e = 0.6$ T (a), 2.0 T (b), and 6.9 T (c) at various values of the nominal oxygen content x_n.

where k is Boltzmann's constant. In Fig. 13 T/Q is displayed as a function of temperature for all oxygen contents considered in this work at $B_e = 0.6$, 2.0, and 6.9 T. The deviations at low and high temperatures are due to quantum creep and thermal depinning, respectively. The crossover from quantum creep to thermally activated creep takes place at $T \approx 6$ K, which is in agreement with values reported in the literature.[4,6,12]

It is, in principle, possible to use the slope μC in the $T/Q(T)$ graphs to identify the pinning regime. For this a value for C is required to evaluate μ. As shown below C can be determined by means of the GIS. The values of μ determined from the slopes μC of the $T/Q(T)$ graphs and the values of C found by means of the GIS (see Sec. VI B) are listed in Table III. Note that the values found for $x_n = 6.85$ are in good agreement with $\mu = 0.95$ at $B_e = 1$ T, reported by Ossandon *et al.*[50]

TABLE III. Experimentally determined values of C and μ.

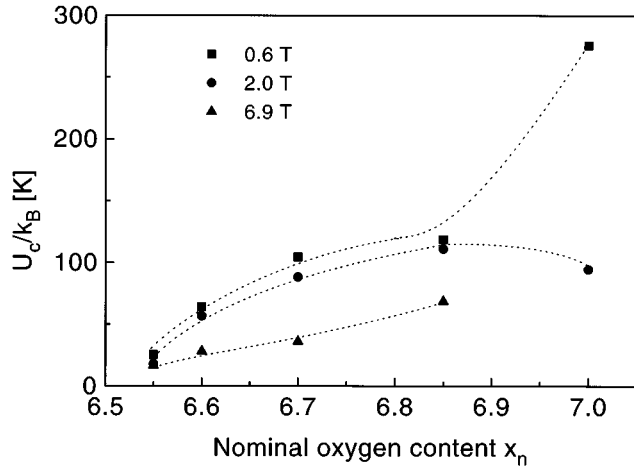| x_n	B_e (T)	C	μ from μC	μ from $U(j)$
7.0	0.6	12	1.17	1.33
7.0	2.0	13	1.52	1.34
6.85	0.6	17	0.87	0.74
6.85	2.0	15	0.95	0.89
6.7	0.6	22	0.33	0.38
6.7	2.0	24	0.27	0.28
6.6	0.6	18	0.34	0.32

FIG. 14. Oxygen content and field dependence of the characteristic pinning energy U_c determined by linear extrapolation to $T = 0$ K of the T/Q values shown in the previous figure.

FIG. 15. Power-law dependence of U_c on the critical current density j_c determined at $B = 0.6$ T (squares) and $B = 2.0$ T (circles). The numbers indicate the oxygen concentration. The open symbols represent data obtained on samples directly after the quench from the annealing temperature to room temperature.

According to these values one would conclude that for $x_n = 6.85$ and $x_n = 7.0$ our sample is in a regime intermediate between single vortex ($\mu = 1/7$) and small bundles ($\mu = 3/2$). The following experimental results are, however, in favor of the single vortex regime. To discuss this point we note that a rather general relation between U_c and j_c has been derived by Schnack *et al.*[16] and Wen *et al.*[51] For example, for a collectively pinned single vortex $U_c \approx j_c \Phi_0 L_c \xi$ where the correlation length $L_c \propto j_c^{-1/2}$ in the 3D regime. This means that $U_c \propto j_c^{1/2}$. In the 2D regime L_c is given by the thickness of the layers and consequently $U_c \propto j_c$. The pinning barrier for a flux bundle is in the collective pinning theory given by $U_c \approx j_c B_e V_B r_p$ where V_B is the volume of the flux bundle and r_p is the range of the potential. A scaling approach has been used to obtain the volume of the flux bundle.[47] This leads finally to a power-law relation between U_c and j_c in the regime of flux bundles.[16] One can generally write

$$U_c(T) \propto [j_c(T)]^p. \tag{26}$$

The values for the exponent p are displayed in the right-hand side of Table II. Although both exponents μ and p are used to relate pinning energies to current densities, their physical origin is very different. The exponent μ describes the relation between the activation energy and the current density when other parameters such as temperature, external field, and oxygen concentration are kept constant. This $U(j)$ relation is partially scanned during a relaxation experiment. The exponent p states that U_c and j_c do not change independently if the external parameters T and B_e or the disorder in the sample are varied.

Extrapolation of the linear part of the T/Q curves to $T = 0$ K gives the values of the characteristic pinning energy U_c, which are shown as a function of oxygen content and magnetic field in Fig. 14. Because U_c and j_c are determined independently it is possible to map U_c as a function of j_c by varying the oxygen concentration and the oxygen ordering of the sample. Data obtained at the same magnetic field can be used for checking Eq. (26). This is displayed in Fig. 15 from which one obtains $p = 0.51$ at $B = 0.6$ T, $p = 0.48$ at $B = 2.0$
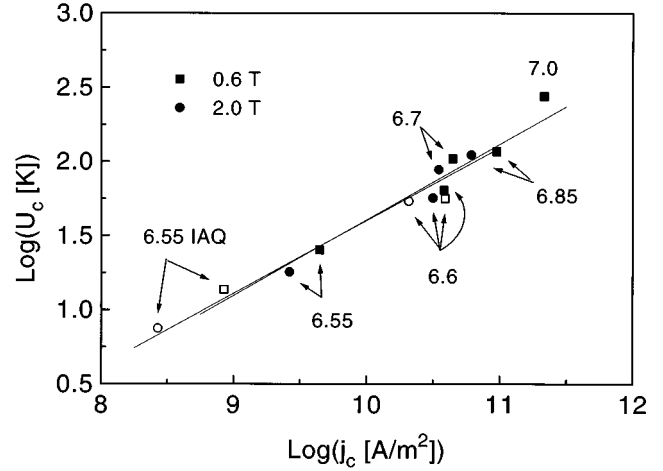
T. At $B = 6.9$ T one finds the value $p = 0.29$. These values imply that below $B = 2$ T the system is certainly in the single vortex regime where each vortex is pinned by the collective action of random weak pinning centers since in this case theory predicts $p = 1/2$ in contrast to $p = -3/2$ and $p = -1/2$ for small and large (super)bundles, respectively. At high fields the system is gradually switching from the single vortex regime to the bundle regime and p decreases ($p = 0.29$ at $B_e = 6.9$ T).

From the data displayed in Fig. 15 one can obtain for the prefactor $\widetilde{C}$ in the power-law relation $U_c = \widetilde{C} j_c^{1/2}$ the value $\widetilde{C} = (5.5 \pm 0.8) \times 10^{-27}$ J m/A$^{1/2}$. Combination of the relation $U_c \approx j_c \Phi_0 L_c \xi$ with the estimate $L_c \approx \epsilon \xi (j_0/j_c)^{1/2}$ derived previously leads directly to $\widetilde{C} \approx 0.25 \Phi_0^{3/2} \xi^{3/2} / \gamma \lambda \mu_0^{1/2}$. However, before applying this relation to experimental results it is important to realize that it is not an exact relation as it is derived from a dimensional estimate. This point is further illustrated by calculating the prefactor $\widetilde{C}$ in a different way. This is done in the next section where U_c and j_c are expressed in terms of the pinning parameter δ. Elimination of this parameter gives finally $\widetilde{C} \approx 0.65 \Phi_0^{3/2} \xi^{3/2} / \gamma \lambda \mu_0^{1/2}$. This result differs from the previously obtained expression for $\widetilde{C}$ by a factor of 2.6.

Using the values $\lambda = 146$ nm, $\xi = 1.6$ nm, and $\gamma = 5.6$ for fully oxidized YBa$_2$Cu$_3$O$_{x_n}$ gives $\widetilde{C} = 1.6 \times 10^{-27}$ J m/A$^{1/2}$. Application of the second equation for $\widetilde{C}$ gives $\widetilde{C} = 4.3 \times 10^{-27}$ J m/A$^{1/2}$, which is in good agreement with the experimentally observed value. However, the ratio $\xi^{3/2} / \gamma \lambda$ is not independent of the oxygen content but decreases with a factor of 2.5 when the oxygen content is decreased from 7.0 to 6.55. A decreasing $\widetilde{C}$ would lead to a downward curvature in the $U_c(j_c)$ diagram, which is not observed here. Considering the uncertainty in the theoretically obtained $\widetilde{C}$ and the experimental values of ξ and λ, we conclude that the agreement with the experimental value is satisfactory.

B. The generalized inversion scheme

A more accurate way to determine the pinning regime and the dimensionality of the system is by using the generalized inversion scheme (GIS) developed by Schnack et al.[16] This is a method to calculate the true critical current density and the activation energy from a set of induced current densities (j_s) and dynamic relaxation rates (Q) measured as a function of temperature at a fixed external field. It also gives information about the exponent p, leading to a determination of the pinning regime and dimensionality.

In contrast to the well-known inversion method of Maley et al.[52] the GIS takes the temperature dependence of U_c and j_c into account, without assuming an explicit analytic expression describing the temperature dependence of U_c and j_c. The starting point of the GIS is the assumption that the temperature and current dependence of the activation energy can be separated in the form

$$U(j_s,T;B_e)=g(T;B_e)\times f(J), \qquad (27)$$

where $J=j_s/j_c(T)$ in which j_c is the true critical current density for which the activation energy vanishes. During a sweep of the applied magnetic field the activation energy is given by[16]

$$U(j,T;B_e)=CkT. \qquad (28)$$

The parameter C can be estimated from the measured data, since at low temperatures g and j_c are nearly temperature independent, leading to

$$C=\lim_{T\to 0}-\frac{1}{Q}\frac{d\ln j_s}{d\ln T}. \qquad (29)$$

It is important to realize that this relation is only valid in the regime of thermally activated flux motion. Direct application of this relation to measured data would lead to an underestimate of C, because $d\ln j_s/d\ln T=(T/j_s)(dj_s/dT)$ becomes zero in the low-temperature limit, while Q remains finite due to quantum creep. As discussed in the previous section, for the extrapolation of Q down to low temperatures, we use the linear temperature dependence of T/Q which extrapolates to a finite value at $T=0$ K. The extrapolation of j_s is more difficult. It might be tempting to use a linear extrapolation of $\ln j_s$, since the data displayed in Fig. 8 suggest that $\ln j_s$ decreases linearly with temperature. However, as discussed recently by Wen et al.,[51] it follows from collective pinning theory that $\ln j_s$ does *not* vary linearly with temperature. The slope $d\ln j_s/dT$ is nearly constant at intermediate temperatures, but increases sharply below $\approx$ 10 K. Unfortunately, this behavior is fully masked by quantum creep. Therefore it follows that extrapolation of the linear temperature dependence of $\ln j_s$ leads to an underestimation of *both* j_s and $d\ln j_s/dT$ and at $T=0$ K and consequently by application of Eq. (29) on experimental data as outlined above, to an underestimation of C. In this work C has been determined by using the fact that at low temperatures $j_c(T)$ and $g(T)$ are to first order independent of the temperature.

A second relation between U_c and j_c is provided by the power-law relation discussed in the previous section. The function $g(T)$ can be associated with U_c leading to
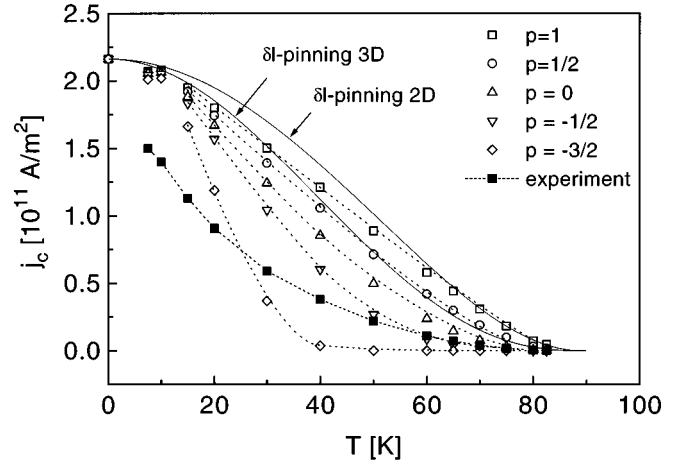

FIG. 16. Temperature dependence of the *true* critical current density j_c obtained by means of the generalized inversion scheme (GIS), using $p=-3/2$, $-1/2$, 0, 1/2, and 1, from data obtained for the YBa$_2$Cu$_3$O$_{x_n}$ film at B_e=0.6 T and x_n = 7.0. The closed symbols represent the measured induced current density j_s. The solid lines give the theoretical predictions based on a model of single vortices pinned by spatial fluctuations of the charge carrier mean free path in three and two dimensions.

$$g(T)\propto U_c(T)\propto[j_c(T)]^p\times G(T), \qquad (30)$$

where the explicit temperature dependence of the activation energy is given by the thermal function $G(T)$ and B_e has been dropped in order to simplify the notation since we consider only data at a given fixed field B_e. This function can be derived from the temperature dependence of the prefactor in the power-law relation between U_c and j_c. Therefore, $G(T)$ depends on the pinning regime (SV, SB, LB) and the dimensionality of the vortices in the sample (see Ref. 51). Following the method outlined by Schnack et al.[16] this leads to

$$\frac{j_c(T)}{j_s(0)}=\exp\left[\int_0^T\frac{CQ(T)(1-d\ln G/d\ln T)+(d\ln j_s/d\ln T)}{1+pCQ(T)}\frac{dT}{T}\right]$$

$$(31)$$

and

$$g(T)=\exp\left[\int_0^T p\frac{CQ(T)+(d\ln j_s/d\ln T)+(1/p)(d\ln G/d\ln T)}{1+pCQ(T)}\right.$$
$$\left.\times\frac{dT}{T}\right]. \qquad (32)$$

Until now, p has been treated as a free parameter. However, from the discussion in the previous section, leading to the power-law relation which defines p, it follows that only the values $p=-3/2$, $-1/2$, 0, 1/2, and 1 are physically meaningful. In the analysis of the experimental data we have only used these values of p. The results of the GIS put more restrictions on p. This is obvious from an inspection of Fig. 16 where the calculated values for j_c are shown together with the measured j_s values. The j_c values are calculated for $p=-3/2$, $-1/2$, 0, 1/2, and 1, respectively. In this example B_e=0.6 T and x_n=7.0. A choice of $p\leq 0$ leads to $j_s>j_c$
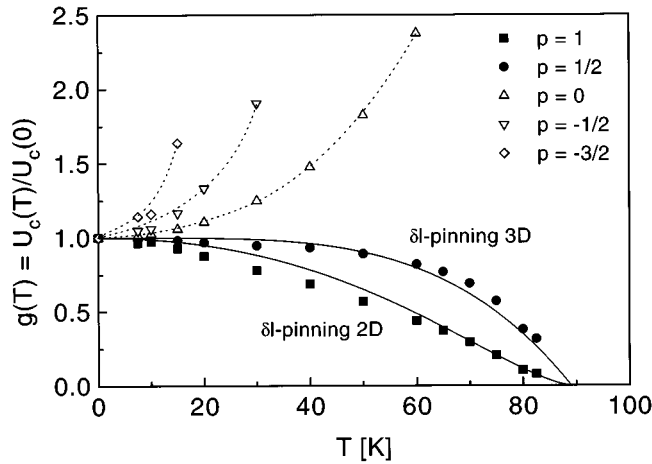
FIG. 17. Normalized temperature dependence of the activation energy obtained from the same dataset as the previous figure. Again the values $p = -3/2, -1/2, 0, 1/2,$ and 1 have been used. The solid and the dashed line give the theoretical prediction based on a model of single vortices pinned by spatial fluctuations of the charge carrier mean free path in three and two dimensions, respectively.

above a certain temperature. This would lead to the conclusion that the sample is in the flux-flow regime. This is in contradiction with the nearly linear dependence of j_s on $\ln(dB_e/dt)$ observed at all temperatures $T < T_{\text{irr}}$. The corresponding $g(T)$ values are shown in Fig. 17. Choosing $p \leq 0$ leads to a rapid divergence of the function $g(T)$. This is physically not acceptable since at $T = T_c$ one expects $U(T_c) = 0$ and thus $g(T_c) = 0$.

Our choice of p is thus limited to $p = 1/2$, corresponding to 3D single vortex pinning and $p = 1$, corresponding to 2D single vortex pinning. From Figs. 16 and 17 it is clear that in *both* cases the temperature dependence of $j_c(T)$ and $U_c(T)$ is in good agreement with the theoretical predictions given by the (3D) and (2D) lines. Therefore, in this case it is not possible to determine the dimensionality of the vortex system by means of the GIS only (although the slightly better agreement for $p = 1/2$ suggests that the 3D single vortex regime is more appropriate). However, in the previous section it has been shown that U_c varies as j_c^p where $p = 0.51$ at $B_e = 0.6$ T and $p = 0.48$ at $B_e = 2$ T. Therefore, we conclude that the system is in the single vortex regime and that vortices behave as 3D objects, despite their short c-axis correlation length.

C. Microscopic origin of pinning

In the framework of collective pinning theory, the pinning potential is due to weak short-range disorder. In type-II superconductors, this disorder arises from spatial fluctuations of the critical temperature and/or the mean free path. These two types of pinning are called δT_c pinning and δl pinning, respectively. Blatter *et al.*[20] use the expansion of the Gor'kov equations near T_c in the clean limit to relate the Ginzburg-Landau parameters α and m to microscopic quantities. These are used to determine the dimensionless pinning parameters δ_α and δ_m for δT_c and δl pinning, respectively. This leads to a temperature dependence of the pinning parameter given by $\delta_\alpha \propto (1-t)^{-1/2}$ and $\delta_m \propto (1-t)^{3/2}$ with

$t = T/T_c$. From the fact that the correlation length varies as $(1-t)^{-1/2}$ for temperatures close to T_c we infer $\delta_\alpha \propto \xi$ and $\delta_m \propto \xi^{-3}$.

In the case of 3D single vortex pinning, Blatter *et al.*[20] showed that all quantities characterizing the collectively pinned vortex line can be expressed in terms of the disorder parameter δ as

$$L_c = \xi \delta^{-1/3} \epsilon^{4/3},$$

$$U_c = \mu_0^{-1} B_c^2 \xi^3 \delta^{1/3} \epsilon^{2/3}, \tag{33}$$

$$j_c = j_0 \delta^{2/3} \epsilon^{-2/3},$$

where ϵ is the mass anisotropy ratio, $B_c = \Phi_0/2\sqrt{2}\pi\lambda\xi$ and $j_0 = 4B_c/3\sqrt{6}\mu_0\lambda$ is the depairing current density. Note that the definition of the disorder parameter used here is different from the more widespread disorder parameter γ defined by $\gamma = f_{\text{pin}}^2 n_i \xi^2$ where f_{pin} is the force exerted on a single flux line by a weak pinning center and n_i is the density of these pinning centers. The last two expresssions of Eq. (33) can be used to derive a δ-independent power-law relation between U_c and j_c:

$$U_c = \left(\frac{B_c^2 \xi^3 \epsilon}{\mu_0 j_0^{1/2}} \right) j_c^{1/2}(T, B_e) = G(T) j_c^{1/2}. \tag{34}$$

The temperature dependence of j_c and U_c is found as follows. As a first step, in the case of 3D single vortex pinning, the thermal function $G(T)$ defined by Eq. (30) can be derived from the temperature dependence of the prefactor in the power-law relation between U_c and j_c in Eq. (34). Comparison of Eqs. (30) and (34) leads straightforwardly to $G(T) \propto B_c^2 \xi^3 j_0^{-1/2}$. Together with $B_c \propto (1-t^2)$, $\xi \propto [(1+t^2)/(1-t^2)]^{1/2}$, and $\lambda \propto (1-t^4)^{-1/2}$ and using $G(0) = 1$ one finds

$$G_{\text{SV}}(t) = (1-t^2)^{-1/4}(1+t^2)^{5/4}. \tag{35}$$

This relation does not depend on the microscopic origin of pinning. The derivation of $G(t)$ proceeds in a similar way in the case of pinning of small and large superbundles (see Ref. 51).

With Eq. (33) it is possible to calculate $j_c(t)/j_c(0)$ once a theoretical model for δ has been chosen. In the case of δT_c pinning one finds

$$\frac{j_c(t)}{j_c(0)} = (1-t^2)^{7/6}(1+t^2)^{5/6} \tag{36}$$

and

$$g(t) = (1-t^2)^{1/3}(1+t^2)^{5/3}. \tag{37}$$

In the case of δl pinning one finds similarly

$$\frac{j_c(t)}{j_c(0)} = (1-t^2)^{5/2}(1+t^2)^{-1/2} \tag{38}$$

and

$$g(t) = (1-t^4). \tag{39}$$

In other cases, the evaluation of the temperature dependence of j_c and U_c proceeds in a similar way.[51] Until recently it
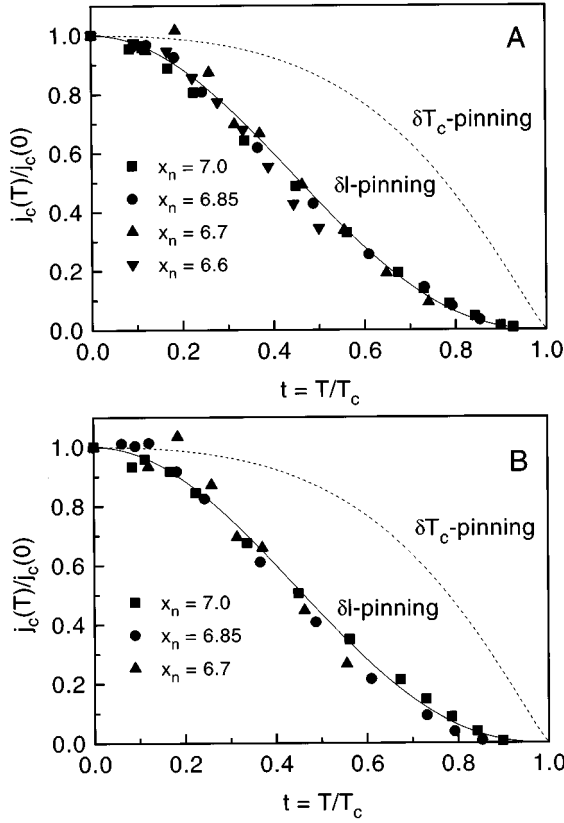
FIG. 18. Critical current density j_c calculated with the GIS, using $p = 1/2$, from data obtained at the $YBa_2Cu_3O_{x_n}$ film at $B_e = 0.6$ T and $x_n \geqslant 6.6$ (a) and $B_e = 2.0$ T and $x_n \geqslant 6.7$ (b). The value $p = 0.5$ corresponds to 3D single vortex pinning. The full line corresponds to pinning due to spatial fluctuations in the charge carrier mean free path (δl pinning) and the dashed line to pinning due to spatial variations in the critical temperature (δT_c pinning).
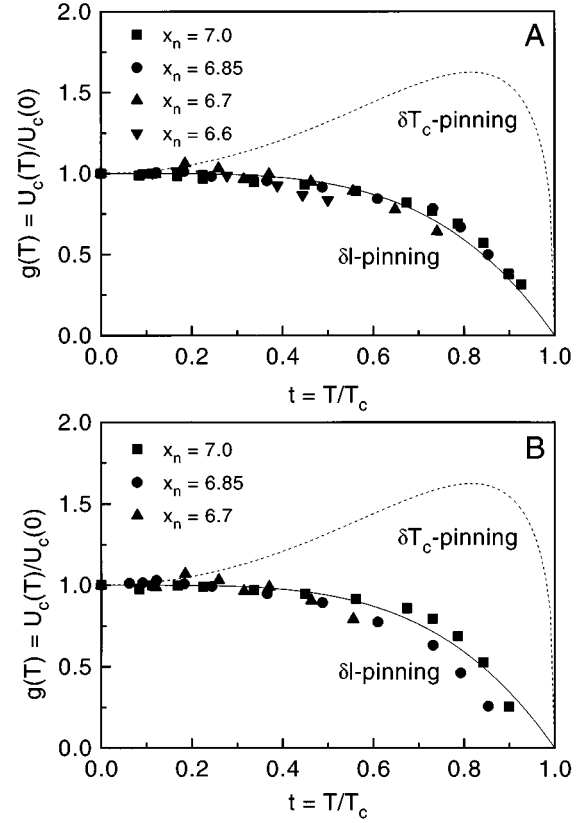
FIG. 19. Temperature dependence of the normalized activation energy, calculated with the GIS, using $p = 1/2$, from data obtained for the $YBa_2Cu_3O_{x_n}$ film at $B_e = 0.6$ T and $x_n \geqslant 6.6$ (a) and $B_e = 2.0$ T and $x_n \geqslant 6.7$ (b). The full line corresponds to δl pinning and the dashed line to δT_c pinning. Note that the theoretical functions given by the solid and the dashed line are fully determined by the value of T_c and do not contain fit parameters.

was not clear which pinning mechanism (δT_c pinning or δl pinning) was the dominant one. The GIS is a very powerful tool to obtain $j_c(t)/j_c(0)$ and $g(t)$, because it does not make any assumption about the type of pinning. The only parameter which has to be specified is the exponent p. From the discussion above it is clear that $YBa_2Cu_3O_{x_n}$ is in the 3D single vortex state, corresponding to $p = 1/2$, leaving no other possibilities.

The GIS has been applied to the values of $j_s(T)$ and $Q(T)$ measured at various nominal oxygen concentrations. The parameter C in Eq. (28) has been obtained from the requirement that the temperature dependence of j_c and U_c is weak at low temperatures. The values of C found in this way, which are diplayed in Table III, are systematically slightly higher than the values of C obtained by application of Eq. (29). The temperature dependence of j_c at $B_e = 0.6$ and 2.0 T is shown in Figs. 18(a) and 18(b), respectively. The corresponding temperature dependence of U_c is shown in Fig. 19(a) ($B_e = 0.6$ T) and Fig. 19(b) ($B_e = 2.0$ T). Only the results for $x_n \geqslant 6.6$ at $B_e = 0.6$ T and $x_n \geqslant 6.7$ at $B_e = 2.0$ T are shown.

The current dependence of the activation energy at $T = 0$ can be calculated from the temperature dependence of j_s/j_c and g, shown in Figs. 18 and 19 in the following way.

The current density $j_s(T)$ measured at a temperature T corresponds to a current density $j_s = j_c(0) \times [j_s(T)/j_c(T)]$ at $T = 0$ K. According to Eq. (28) the activation energy $U[j_s(T),T]$ at a temperature T is given by $U(j) = CkT$. The corresponding activation energy $U(j_s,0)$ is then evaluated from $U[j_s(T),T] = g(T) \times U(j_s,0)$. Measurements of j_s and $U(j_s,T)$ at various T are thus mapped onto a single curve, where the points at low current density are deduced from measurements at high temperature and vice versa. The $U(j,T=0)$ curves for $x_n = 6.6$, 6.7, 6.85, and 7.0 at $B_e = 0.6$ T and $x_n = 6.7$, 6.85, and 7.0 at $B_e = 2.0$ T are shown in Figs. 20(a) and 20(b), respectively. The presentation in double logarithmic coordinates clearly shows that $U(j)$ cannot be written as $U \propto j^{-\tilde{\mu}}$ with a single valued, i.e., current independent exponent $\tilde{\mu}$ which is different from the exponent μ defined by Eq. (23). The solid lines are fits to Eq. (23) which takes the condition $U(j_c) = 0$ into account. For $x_n = 6.85$ and 7.0 the $U(j)$ values obtained at high temperatures where T/Q decreases with increasing temperature (see Fig. 13) have been excluded from the fitting procedure. In contrast to van der Beek et al.[53] who uses $U \propto j^{-\tilde{\mu}}$ instead of Eq. (23) we find that $U(j)$ can be satisfactorily described by a single, current independent value of μ. The values of μ,
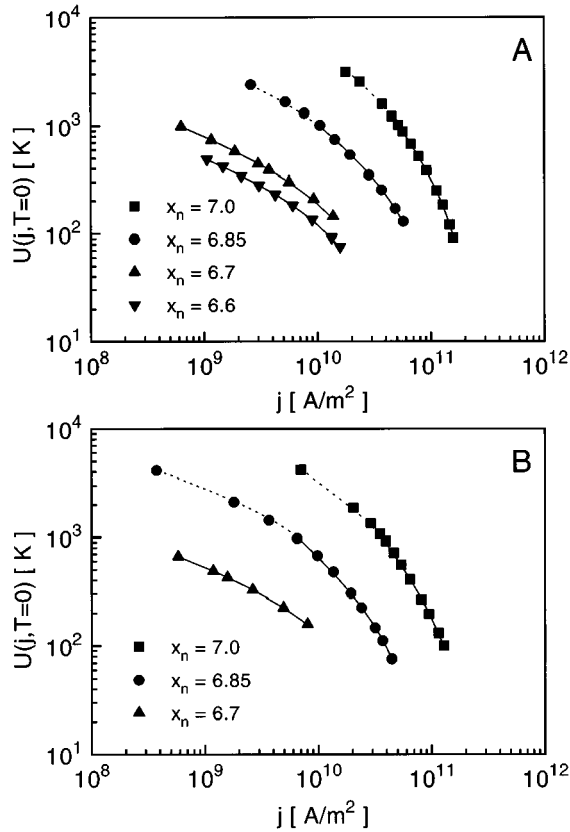
FIG. 20. Current dependence of the activation energy $U(j,T=0)$ for $x_n=$ 6.6, 6.7, 6.85, and 7.0 at $B_e=0.6$ T (a) and for $x_n=$ 6.7, 6.85, and 7.0 at $B_e=2.0$ T. The solid lines are fits to Eq. (23), whereas the dotted lines are a guide to the eye. For $x_n=6.85$ and 7.0 the $U(j)$ values obtained from measurements at the highest temperatures have been excluded from the fit.

VII. CONCLUSIONS

In this work the induced current density j_s and dynamic relaxation rate Q of an $YBa_2Cu_3O_{x_n}$ film with adjustable oxygen content have been measured as a function of temperature and magnetic field. The relaxation rate does not extrapolate to zero at $T=0$ K which is caused by quantum creep of the vortices through the energy barriers separating metastable vortex configurations. We observe that the quantum creep rate and the normal-state resistivity increase as the oxygen content is decreased. However, the quantum creep rate is not proportional to the normal-state resistivity which is predicted by collective pinning theory. This behavior cannot be explained by taking the influence of the correlation length L_c into account, since this is only weakly dependent on the oxygen content. The weak variation of $Q(0)$ with $\rho_n(0)$ indicates that quantum creep occurs in a transition regime between dissipative tunneling and Hall tunneling. This implies that the average direction of vortex motion is neither parallel nor perpendicular to the current. The process of quantum creep shifts towards the dissipative limit for decreasing oxygen content. The weak increase of $Q(0)$ with magnetic field indicates that quantum creep is certainly not involving vortex bundles.

An independent determination of j_c and the characteristic pinning energy U_c shows that the system remains in the single vortex limit at higher temperatures, where the vortices move due to thermal activation over the energy barriers. This is shown in more detail by calculating the true critical current density and the thermal activation energy by means of the generalized inversion scheme. This procedure diverges if one assumes pinning of vortex (super)bundles. For $x_n\geqslant6.6$ at $B_e=0.6$ T and for $x_n\geqslant6.7$ at $B_e=2.0$ T the calculated temperature dependences of the true critical current density and the activation energy are in good agreement with theoretical predictions, showing that in these cases the pinning is due to fluctuations in the charge carrier mean free path. For lower oxygen contents and higher magnetic fields the agreement between the results of the inversion and the theoretical predictions becomes less good. This is possibly explained by the presence of thermal fluctuations, since in these cases the activation energy is strongly reduced. We have observed that the activation energy and the critical current density systematically decrease with decreasing oxygen content. This leads to the conclusion that oxygen vacancies are not the main source of pinning in $YBa_2Cu_3O_{x_n}$ films.

displayed in Table III are in good agreement with the values of μ previously determined from the slope μC of T/Q versus T.

From Figs. 18 and 19 it is clear that $j_c(T)/j_c(0)$ and $g(T)$ are in remarkably good agreement with the theoretical predictions based upon δl pinning. The agreement between the theoretical predictions Eqs. (38) and (39) and the calculated values of $j_c(T)/j_c(0)$ and $g(T)$ gradually breaks down at lower oxygen contents and higher magnetic fields. In these cases $U_c(0)$ is lower than ≈60 K and the effect of thermal fluctuations when T approaches T_{irr} is not negligible any more. The predictions for δT_c pinning are in total disagreement with the observations. This result has also been obtained on $YBa_2Cu_3O_7$ and $YBa_2Cu_4O_8$ films[54] and recently on a twin-free $DyBa_2Cu_3O_{7-\delta}$ single crystal.[55]

The disorder parameter δ can be evaluated from Eq. (33) leading to $\delta=\gamma^{-1}(j_c/j_0)^{3/2}$ where j_0 is given by $j_0=\Phi_0/(3\sqrt{3}\pi\mu_0\lambda^2\xi)$. The variation of δ with oxygen content is calculated from the values of λ, ξ, γ, and j_c given in Table I This leads to $\delta=3.5\times10^{-3}$ for $x_n=7.0$ and to $\delta=1.6\times10^{-5}$ for $x_n=6.55$. Furthermore it is found that δ decreases monotonically with decreasing oxygen content. This is somewhat surprising since disorder is expected to be proportional to the number of defects.

*Present address: Materials Science Division, Argonne National Laboratory, Argonne, Ilinois 60439.

†Present address: Montell Polyolefins, Centre Ricerche ''G. Natta,'' P. Le P. to G. Donegani 12, 44100 Ferrara, Italy.

[1] A. C. Mota, A. Pollini, P. Visani, K. A. Müller, and J. G. Bednorz, Phys. Scr. **37**, 823 (1988).

[2] P. W. Anderson and Y. B. Kim, Rev. Mod. Phys. **36**, 39 (1964).

[3] R. Griessen, Physica C **172**, 441 (1991).

[4] L. Fruchter, A. P. Malozemoff, I. A. Campell, J. Sanchez, M. Konczykowski, R. Griessen, and F. Holtzberg, Phys. Rev. B **43**, 8709 (1991).

[5] S. Uji, H. Aoki, S. Takebayashi, M. Tanaka, and M. Hashimoto, Physica C **207**, 112 (1993).

[6] A. C. Mota, G. Juri, P. Visani, A. Pollini, T. Teruzzi, and K. Aupke, Physica C **185-189**, 343 (1991).

[7] A. Hoekstra, J. C. Martinez, and R. Griessen, Physica C **235-240**, 2955 (1994).

[8] G. T. Seidler, T. F. Rosenbaum, K. M. Beauchamp, H. M. Jaeger, C. W. Crabtree, U. Welp, and V. M. Vinokur, Phys. Rev. Lett. **74**, 1442 (1995).

[9] S. Moehlecke and Y. Kopelevich, Physica C **222**, 149 (1994).

[10] D. Prost, L. Fruchter, I. A. Campbell, N. Motohira, and M. Konczykowski, Phys. Rev. B **47**, 3457 (1993).

[11] K. Aupke, T. Teruzzi, P. Visani, A. Amann, and A. C. Mota, Physica C **209**, 255 (1993).

[12] A. Garcia, X. X. Zhangh, A. M. Testa, D. Fiorani, and J. Tejada, J. Phys. Condens. Matter **4**, 10 341 (1992).

[13] J. Tejada, E. M. Chudnovsky, and A. Garcia, Phys. Rev. B **47**, 11 552 (1993).

[14] G. Blatter, V. B. Geshkenbein, and V. M. Vinokur, Phys. Rev. Lett. **66**, 3297 (1991).

[15] G. Blatter and V. B. Geshkenbein, Phys. Rev. B **47**, 2725 (1993).

[16] H. G. Schnack, R. Griessen, J. G. Lensink, and H.-H. Wen, Phys. Rev. B **48**, 13 178 (1993).

[17] A. O. Caldeira and A. J. Leggett, Phys. Rev. Lett. **46**, 211 (1981).

[18] R. Griessen, J. G. Lensink, and H. G. Schnack, Physica C **185-189**, 337 (1991).

[19] J. Bardeen and M. J. Stephen, Phys. Rev. **140**, 1197A (1965).

[20] G. Blatter, M. V. Feigel'man, V. B. Geshkenbein, A. I. Larkin, and V. M. Vinokur, Rev. Mod. Phys. **66**, 1125 (1994).

[21] M. V. Feigel'man, V. B. Geshkenbein, A. I. Larkin, and S. Levit, JETP Lett. **57**, 711 (1993).

[22] N. B. Kopnin and V. E. Kravtsov, Sov. Phys. JETP **44**, 861 (1976).

[23] N. B. Kopnin and M. M. Salomaa, Phys. Rev. B **44**, 9667 (1991).

[24] M. J. Stephen, Phys. Rev. Lett. **72**, 1534 (1994).

[25] A. O. Caldeira and A. J. Leggett, Ann. Phys. (N.Y.) **149**, 374 (1983).

[26] B. Wuyts, Z. X. Gao, S. Libbrecht, M. Maenhoudt, E. Osquiguil, and Y. Bruynseraede, Physica C **203**, 235 (1992).

[27] E. Osquiguil, M. Maenhoudt, B. Wuyts, and Y. Bruynseraede, Appl. Phys. Lett. **60**, 1627 (1992).

[28] P. K. Gallagher, Adv. Ceram. Mater. **2**, 632 (1987).

[29] S. Libbrecht, Ph. D. thesis, Katholieke Universiteit Leuven, Belgium, 1994.

[30] J. G. Ossandon, J. R. Thompson, D. K. Christen, B. C. Sales, H. R. Kerchner, J. O. Thompson, Y. R. Sun, K. W. Lay, and J. E. Tkaczyk, Phys. Rev. B **45**, 12 534 (1992).

[31] E. C. Jones, D. K. Christen, J. R. Thompson, R. Feenstra, S. Zhu, D. H. Lowndes, J. M. Philips, M. P. Siegal, and J. D. Budai, Phys. Rev. B **47**, 8986 (1993).

[32] M. Qvarford, K. Heeck, J. G. Lensink, R. J. Wijngaarden, and R. Griessen, Rev. Sci. Instrum. **63**, 5726 (1992); see also R. Griessen, M. J. G. Lee, and D. J. Stanley, Phys. Rev. B **16**, 4385 (1977).

[33] M. R. Koblischka, Th. Schuster, B. Ludescher, and H. Kronmüller, Physcia C **190**, 557 (1992).

[34] Th. Schuster, M. R. Koblischka, H. Kuhn, and H. Kronmüller, J. Appl. Phys. **74**, 3307 (1993).

[35] M. R. Koblischka, R. J. Wijngaarden, D. G. de Groot, R. Griessen, A. A. Menovsky, and T. W. Li, Physica C **249**, 339 (1995).

[36] H. G. Schnack, R. Griessen, J. G. Lensink, C. J. van der Beek, and P. H. Kes, Physica C **197**, 337 (1992).

[37] E. H. Brandt, Phys. Rev. Lett. **74**, 3025 (1995).

[38] H. P. Wiesinger, F. M. Sauerzopf, and H. W. Weber, Physica C **203**, 121 (1992).

[39] M. Jirsa, L. Půst, H. G. Schnack, and R. Griessen, Physica C **207**, 85 (1993).

[40] L. Půst, M. Jirsa, R. Griessen, and H. G. Schnack, Appl. Supercond. **1**, 835 (1993).

[41] L. Půst, J. C. Martinez, A. J. J. van Dalen, A. Hoekstra, H.-H. Wen, and R. Griessen, in *Critical Currents in Superconductors*, edited by H. W. Weber (World Scientific, Singapore, 1994), p. 240.

[42] K. E. Gray, D. H. Kim, B. W. Veal, G. T. Seidler, T. F. Rosenbaum, and D. E. Farrell, Phys. Rev. B **45**, 10 071 (1992).

[43] B. Janossy, D. Prost, S. Pekker, and L. Fruchter, Physica C **181**, 51 (1991).

[44] M. Däumling, Physica C **183**, 293 (1991).

[45] A. J. J. van Dalen, R. Griessen, J. C. Martinez, P. Fivat, J.-M. Triscone, and Ø. Fischer, Phys. Rev. B, **53**, 896 (1996).

[46] L. L. Daemen, L. N. Bulaevskii, M. P. Maley, and J. Y. Coulter, Phys. Rev. B **47**, 11 291 (1993).

[47] M. V. Feigel'man, V. B. Geshkenbein, A. I. Larkin, and V. M. Vinokur, Phys. Rev. Lett. **63**, 2303 (1989).

[48] E. Zeldov, N. M. Amer, G. Koren, A. Gupta, M. V. McElfresh, and R. J. Gambino, Phys. Rev. Lett. **62**, 3093 (1989).

[49] H.-H. Wen, R. Griessen, D. G. de Groot, B. Dam, and J. Rector, J. Alloys Compounds **195**, 427 (1993).

[50] J. G. Ossandon, J. R. Thompson, D. K. Christen, B. C. Sales, Yangren Sun, and K. W. Lay, Phys. Rev. B **46**, 3050 (1992).

[51] H.-H. Wen, H. G. Schnack, R. Griessen, B. Dam, and J. Rector, Physica C **241**, 353 (1995).

[52] M. P. Maley, J. O. Willis, H. Lessure, and M. E. McHenry, Phys. Rev. B **42**, 2639 (1990).

[53] C. J. van der Beek, P. H. Kes, M. P. Maley, M. J. V. Menken, and A. A. Menovsky, Physica C **195**, 307 (1992).

[54] R. Griessen, Wen Hai-hu, A. J. J. van Dalen, B. Dam, J. Rector, H. G. Schnack, S. Libbrecht, E. Osquiguil, and Y. Bruynseraede, Phys. Rev. Lett. **72**, 1910 (1994).

[55] A. J. J. van Dalen, M. R. Koblischka, R. Griessen, M. Jirsa, and G. Ravi Kumar, Physica C **250**, 265 (1995).